Supplementary Information

Fabrication Process Flow

A more detailed process flow for the nDS*ab* is detailed in Table S1, including the specific process conditions, the equipment model designations and manufacturers, and the suppliers for all materials. Figure S1 schematically depicts the 11 die positions scanned using atomic force microscopy (AFM) to determine the nanotrench depth prior to anodically bonding the Pyrex cap. Scanning electron micrographs of the cross section of the nDS is displayed in Figure S2.

Table S1: The process flow for the 22nm anodically bonded nanochannels

Process Step:	Conditions:
Dry thermal oxidation of pad layer for selective oxidation mask	950°C 6 L/min O_2 Layer thickness: 65 nm
LPCVD of silicon nitride for selective oxidation mask	800°C 20 sccm H_2SiCl_2 70 sccm NH_3 70 mTorr Layer thickness: 65 nm
Photolithography for nanotrenches	EVG620 Contact Aligner (EV Group) AZ 5209 as positive resist (Clariant Corp.) spun at 5000 rpm to a thickness of ~900 nm
Reactive ion etch through silicon nitride down to pad oxide layer for nanotrenches	Plasma-Therm 790 (Plasma-Therm, LLC) 40 sccm CHF_3 3 sccm O_2 40 mTorr 400 Watts Etch depth: slightly over 65nm
Buffered oxide etch through pad oxide for nanotrenches	6:1 buffered oxide etch (Capitol Scientific, Inc.)
Piranha clean of resist	H_2SO_4 (96%) : H_2O_2 (30%) = 2:1 (KMG Chemicals, Inc. : Ultra Pure Solution, Inc.)
HF dip to remove chemically grown oxide from patterns	H_2O : HF (49%) = 20:1 (KMG Chemicals, Inc.)
Selective dry thermal oxidation of nanotrenches	950°C 6 L/min O_2 Layer thickness: 50 nm
HF strip of nitride mask and selectively grown oxide	H_2O : HF (49%) = 20:1 (KMG Chemicals, Inc.)
LPCVD of silicon dioxide hard mask for Bosch etch of the inlet micro- and macrochannels	600°C 70 sccm SiH_4 40 sccm O_2 Layer thickness: 1 µm
Thinning of silicon dioxide hard mask on the device layer side of the SOI substrate to 400nm for the Bosch etch of the inlet microchannels	Plasma-Therm 790 40 sccm CHF_3 3 sccm O_2 75 mTorr 450 Watts Etch depth: 600 nm
Photolithographic patterning of the inlet macrochannels	EVG620 Contact Aligner, double side alignment NR9-3000P (Futurrex, Inc.) negative resist spun to ~3 µm thick
Reactive ion etch through silicon dioxide hard mask for the inlet macrochannels	Plasma-Therm 790 40 sccm CHF_3 3 sccm O_2 75 mTorr

<table>
<tr><td></td><td>450 Watts
Etch depth: 1 μm</td></tr>
<tr><td>Piranha clean of resist</td><td>H_2SO_4 (96%) : H_2O_2 (30%) = 2:1
(KMG Chemicals, Inc. : Ultra Pure Solution, Inc.)</td></tr>
<tr><td>Photolithographic patterning of the inlet microchannels</td><td>EVG620 Contact Aligner
NR9-1000P (Futurrex Inc.) negative resist spun at 3000 rpm to a thickness of ~1 μm</td></tr>
<tr><td>Reactive ion etch through silicon dioxide hard mask for the inlet microchannels</td><td>Plasma-Therm 790
40 sccm CHF_3
3 sccm O_2
75 mTorr
450 Watts
Etch depth: 400 nm</td></tr>
<tr><td>Piranha clean of resist</td><td>H_2SO_4 (96%) : H_2O_2 (30%) = 2:1
(KMG Chemicals, Inc. : Ultra Pure Solution, Inc.)</td></tr>
<tr><td>HF dip to remove chemically grown oxide from patterns</td><td>H_2O : HF (49%) = 20:1
(KMG Chemicals, Inc.)</td></tr>
<tr><td>Bosch etch for the inlet microchannels through 30μm device layer</td><td>Plasma-Therm Versaline Generation 2 Deep Silicon Etcher (Plasma-Therm, LLC)
<table>
<tr><td>Number of cycles</td><td>52</td></tr>
<tr><td>Polymer deposition:
C_4F_8 75 sccm
Ar 30 sccm
20 mTorr
RF forward bias power 1 Watts
ICP RF power 1200 Watts</td><td>2 seconds</td></tr>
<tr><td>Polymer removal from bottom of trench
SF_6 100 sccm
Ar 30 sccm
29 mTorr
RF forward bias power 10 Watts
ICP RF power 1200 Watts</td><td>4 seconds</td></tr>
<tr><td>Silicon etch
SF_6 200 sccm
Ar 30 sccm
46 mTorr
RF forward bias power 12 Watts
ICP RF power 1200 Watts</td><td>3 seconds</td></tr>
</table></td></tr>
<tr><td>Bosch etch for the inlet macrochannels through 500μm handle wafers</td><td>Plasma-Therm Versaline Generation 2 Deep Silicon Etcher
<table>
<tr><td>Number of cycles</td><td>284,
then 284,
then 90
until finished</td></tr>
<tr><td>Polymer deposition:
C_4F_8 75 sccm
Ar 30 sccm
20 mTorr
RF forward bias power 1 Watts
ICP RF power 1200 Watts</td><td>2 seconds,
then
2 seconds,
then
2 seconds</td></tr>
<tr><td>Polymer removal from bottom of trench
SF_6 100 sccm
Ar 30 sccm
29 mTorr
RF forward bias power 10 Watts
ICP RF power 1200 Watts</td><td>4 seconds,
then
6 seconds,
then
7 seconds</td></tr>
<tr><td>Silicon etch
SF_6 200 sccm
Ar 30 sccm
46 mTorr
RF forward bias power 12 Watts
ICP RF power 1200 Watts</td><td>3 seconds,
then
2 seconds,
then
2 seconds</td></tr>
</table></td></tr>
</table>

Piranha clean of sample to remove any Bosch polymer from the patterned SOI substrate	H_2SO_4 (96%) : H_2O_2 (30%) = 2:1 (KMG Chemicals, Inc. : Ultra Pure Solution, Inc.)
HF dip to strip LPCVD silicon dioxide masks and exposed buried oxide layer through the inlet macrochannels	H_2O:HF(49%) = 10:1 (KMG Chemicals, Inc.)
AFM of nanotrenches (NanoMan VS Scanning Probe Microscope, Veeco Instruments, Inc.)	Scan size: 16 µm Aspect ratio: 8:1 Samples per line: 256 Scan rate: 0.3 Hz Lines: 32 Number of nanotrenches scanned per wafer: 11 (see supplementary Figure. S1)
Nanochannel formation by the anodic bonding of Pyrex to the device layer of the SOI substrate	EVG520IS Semi-Automated Wafer Bonding System (EV Group) 1. High vacuum 2. Heat to 310°C at 20°C/min 3. Pull out separation flags 4. Apply high voltage electrode contact of -1000 V for 20 minutes 5. Purge chamber 6. Cool down
Thinning of the Pyrex capping wafer by lapping	Ron Kehl Engineering, San Jose, CA SOI/Pyrex wafer stacks were reversibly bonded to 6 inch in diameter ¼ inch thick stainless steel backing plates using an Alcowax (Nikka Seiko Co., LTD, stripped in isopropyl alcohol) 1. 15 µm diamond slurry for ~480 µm removal in 10 to 20 minute cycles 2. Cerium oxide for final polish Intermediate Pyrex thicknesses were determined by mechanical drop gauge. Final Pyrex thickness was determined by reflectometry Final Pyrex thickness: < 20 µm
Strip of residual bonding wax	Isopropyl alcohol
Deposition of electroplating seed layer	Electron Beam Evaporator (CHA Industries) Cr deposited at a rate of ~0.5 Å/sec at ~27% power Au deposited at a rate of ~1.1 Å/sec at ~37.6% power Final thickness Cr: 10 nm Final thickness Au: 50 nm
Photolithography of outlet microchannels for electrochemical deposition template	EVG620 Contact Aligner Megaposit SPR220-4.5 positive resist (Rohm and Haas Company) spun at 2500 rpm Stripped in acetone
Electrochemical deposition of nickel	Nickel Plating Kit (Caswell Inc.) Includes: 1. Plating tanks 2. Nickel sulphate/Nickel chloride crystals and saccharin based brightener 3. Nickel anodes 4. Degreaser (unnecessary here) 5. Ceramic heaters 6. Thermostat 7. Pump for filtering and agitation Final thickness: 4 µm
Removal of seed layer from inside outlet microchannel patterns	Etchants obtained from Transene Company, Inc. 1. Gold Etchant TFA (KI-I_2 complex) 2. Chromium Etchant TFD (ceric sulfate, nitric acid, sulphuric acid, water)
Deep dielectric etch of the outlet microchannels	Plasma-Therm Versaline Generation 2 Deep Dielectric Etcher 1. Time 1860 seconds 2. SF_6: 45 sccm

	3. O_2: 5 sccm 4. Ar: 20 sccm 5. 10 mTorr 6. RF forward bias: 400 Watts 7. RF ICP bias: 1500 Watts Etch depth: > 20 μm
Removal of nickel mask and seed layer	Etchants obtained from Transene Company, Inc. 1. Nickel Etchant Type I ($FeCl_3$.$6H_2O$, HCl, H_2O) 2. Gold Etchant TFA (KI-I_2 complex) 3. Chromium Etchant TFD (ceric sulfate, nitric acid, sulphuric acid, water)
Dicing to separate individual die	Disco 321 Dicing Saw UV release tape (ProFilm™ DU177E, Advantek, Inc.)
Optional: Nanochannel length adjusters:	
LPCVD of silicon nitride for selective oxidation mask	800°C 20 sccm H_2SiCl_2 70sccm NH_3 70 mTorr Layer thickness: 65 nm
Photolithography for nanochannel length adjusters	EVG620 Contact Aligner (EV Group) AZ 5209 as positive resist (Clariant Corp.) spun at 5000 rpm to a thickness of ~900 nm
Reactive ion etch through silicon nitride for nanochannel length adjusters	Plasma-Therm 790 (Plasma-Therm, LLC) 40 sccm CHF_3 3 sccm O_2 40 mTorr 400 Watts Etch depth: 65 nm
Potassium hydroxide etch of nanochannel length adjusters to depth of ~1 μm or Wet thermal oxidation of nanochannel length adjusters to depth of 0.5 to 1 μm	KOH (45%) @ 80°C (Capitol Scientific, Inc.) 1050°C 3 L/min H_2
HF dip of sample to remove the silicon nitride mask and the selectively grown wet oxide	H_2O : HF (49%) = 20:1 (KMG Chemicals, Inc.)

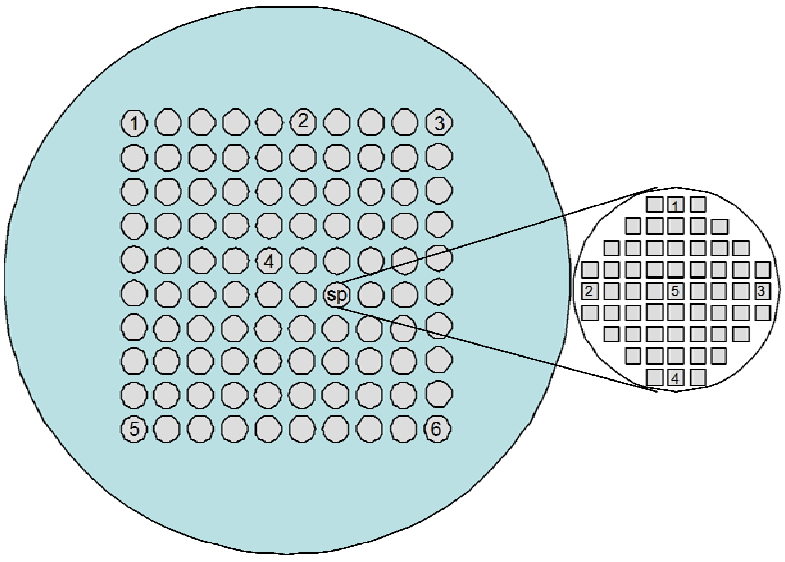

Figure S1. The wafer position of the die whose nanotrenches were sampled by atomic force microscopy prior to Pyrex capping. 11 scans were recorded for each wafer.

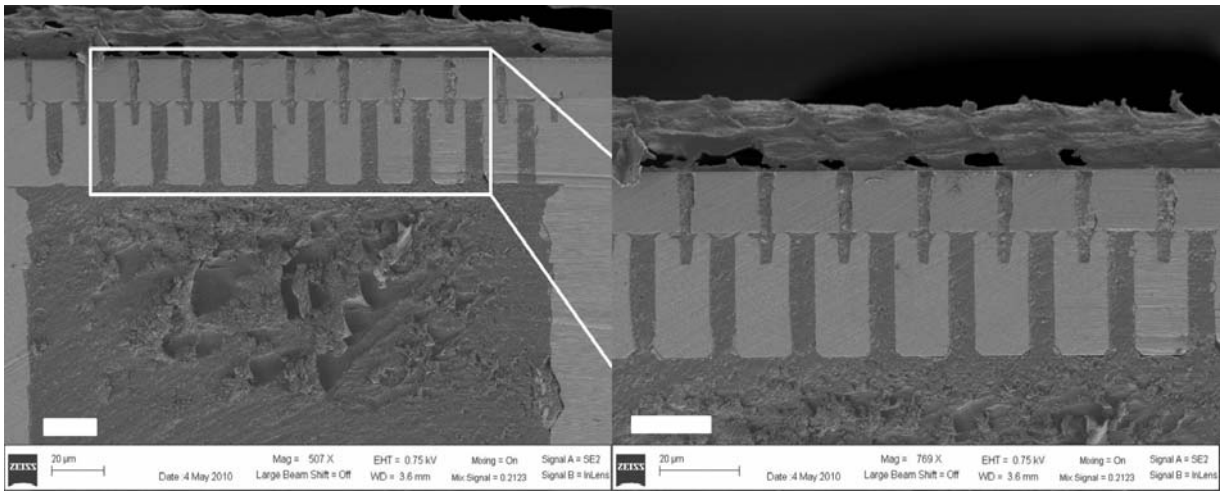

Figure S2. Scanning electron micrographs of the cross section of the nDS showing the top of the inlet macrochannel, the inlet microchannels, the nanochannel length adjusters, and the outlet microchannels. The samples were embedded using Spurr epoxy resin[1], diced along the nanochannel length and surface polished using diamond lapping films of 1 µm, 0.5 µm, and finally 0.1 µm. The roughness of the epoxy in the macrochannel and the striations on the silicon are due to the lapping process. The outlet microchannels (at top) were over etched to insure that the nanochannel length adjusters were effectively interfaced. The epoxy resin helped to prevent damage to the fine structure of the membrane but did not eliminate the damage completely, especially around the length adjusters and the outlet microchannels. The outlet microchannels are smaller in cross section than the inlet microchannels owing to the resist mesas used to template the nickel electroplating process had an aspect ratio of 1 to 1 at 4.5 µm in height and therefore had a significant taper. The material above the Pyrex is copper tape used to reduce charging during electron scanning.

Testing Apparatus

Gas Test

Table S2 lists the equipment, with suppliers, which comprised the gas testing apparatus. Figure S3 depicts the gas testing apparatus.

Table S2: The gas testing system components

High purity nitrogen tank (99.9999%)	Matheson Tri-Gas®
Dual stage regulator	Matheson Tri-Gas®, 3120-580
Pressure transducer	Omegadyne Inc., PX01C1-200G5T
Gas filter	Matheson Tri-Gas®
Precision o-rings	Apple Rubber, Lancaster, NY
Hand-held multimeter	Fluke 77IV Multimeter
Digital multimeter	Agilent model 34410A 6½ digit multimeter Agilent Technologies, Santa Clara, CA
Stainless steel used for manufacturing the gas test clamping system and membrane holder	Type SS316L
High pressure regulator for burst testing	Victor VIC0386-0814 with a range of 0-4.137MPa

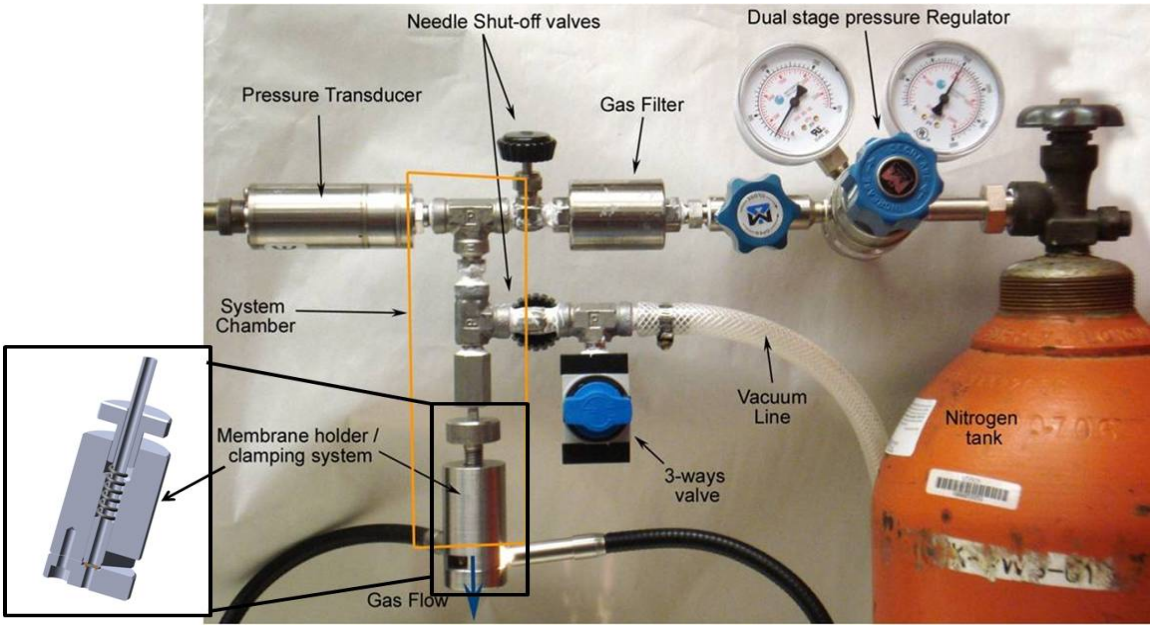

Figure S3. The gas test apparatus.

Gas Test Reproducibility

The reproducibility of the system was also verified by repetitively (10 times) performing the gas testing with a nanochanneled device[2]. Figure S4 shows the comparison of the experimental results. The standard deviation of the experimental results was found to be always smaller than $1.13*10^{-4}$ % which value was calculated in respect of the mean of data. The skew of the population of data was calculated to evaluate the normality of the data distribution. The small value of the skew (-0.14) indicates that the data presents a negligible deviation from a Gaussian distribution. The differences among experimental results were associated to the noise of the testing system. The results confirm that the noise is significantly smaller than the nominal repeatability limit of the pressure transducer (± 0.35 %).

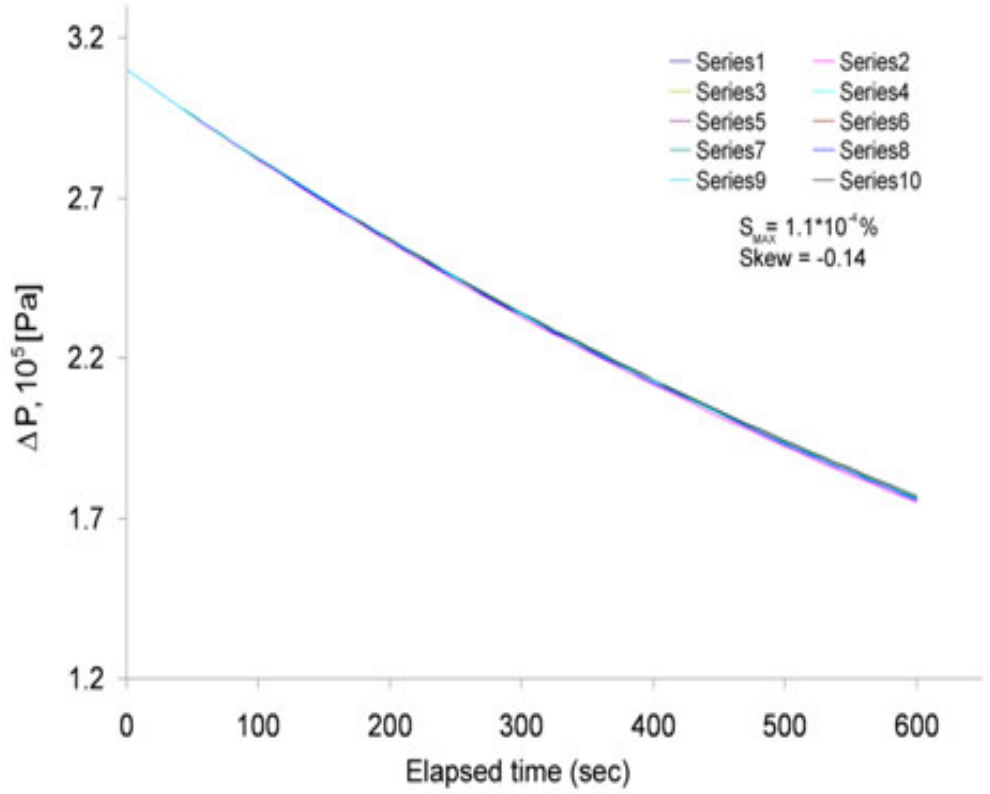

Figure S4 – Results of the experimental pressure testing performed 10 times on the same membrane. The value of the maximum standard deviation S and skew of the data distribution are also listed.

Gas Test Experimental Data Interpolation

The pressure drop is well described by a single exponential decay, consistent with the solution to a one-dimensional transient problem. The collected pressure data were thus fitted with an exponential function $p(t) = k \cdot e^{-Dt}$ (correlation coefficient R_c always >0.999). The interpolation was performed to resample each curve and in a time range of 60 s starting from a relative pressure of k = 0.31 MPa with Figure S5 showing the results from a single nDS membrane gas test.

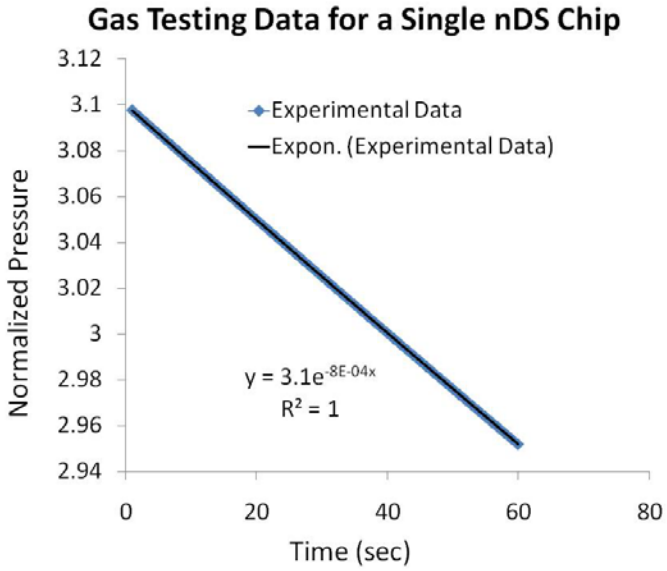

Figure S5. The results of a gas test for a single nDS membrane.

Diffusion Test

Table S3 details the equipment, with suppliers, used for building the diffusion testing apparatus.

Tabel S3: Diffusion testing system components

Stainless steel used for manufacturing both of the chamber designs for the diffusion testing	Type SS316L
Precision o-rings	Apple Rubber, Lancaster, NY
Silicon rubber caps	Mocap, Inc., St. Louis, MO
UV macro-cuvette	BrandTech Scientific, Inc., Essex, CT
UV-curing epoxy resin	OG116-31 Epoxy Technologies, Billerica, MA
A FreeStyle Lite® Blood Glucose Monitoring System	Abbott Laboratories
Life Science UV/Vis Spectrophotometer	Beckman Coulter DU®730
Spectrophotometer used for the FITC-dextran measurements	BMG Labtech GmbH

UV Absorbance Standard Curve

Figure S6 shows as an example, the calibration curve for a UV diffusion test with the diffusion chamber D1.

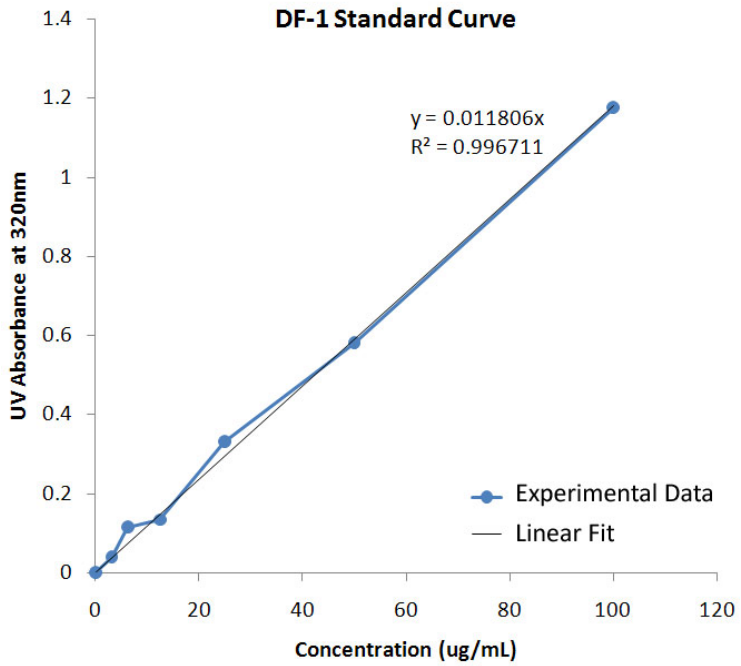

Figure S6. Calibration curve used for the UV diffusion testing of DF-1 in chamber D1

Finite Element Analysis (FEA)

A finite element model was developed for the analysis and prediction of the diffusive transport in the nDS membranes. The model considers unsteady diffusion. The simplifications consist in assuming that concentration is uniform within both inlet and outlet reservoirs and that the concentration field is the same for any inlet or outlet microchannels, at any time. 2D and 1D elements are used for microchannels and nanochannels, respectively. The finite element model is generated based on geometric, material and mesh parameters. The governing balance equation based on Fick's law of diffusion (1) can be written as

$$-\frac{\partial c}{\partial t}+\nabla^T\left(D\nabla c\right)=0 \qquad (1)$$

This equation is transformed to the finite element format by a standard Galerkin procedure and time integration is performed using a selected time step Δt. The incremental-iterative equation of mass balance for a finite element and time step n has the form[3]:

$$\left(\frac{1}{\Delta t}\mathbf{M}+{}^{n+1}\mathbf{K}^{(i-1)}\right)\Delta\mathbf{C}^{(i)}={}^{n+1}\mathbf{Q}^{S(i-1)}-{}^{n+1}\mathbf{K}^{(i-1)}\,{}^{n+1}\mathbf{C}^{(i-1)}-\frac{1}{\Delta t}\mathbf{M}\left({}^{n+1}\mathbf{C}^{(i-1)}-{}^{n}\mathbf{C}\right) \qquad (2)$$

where terms of the matrices $\mathbf{M}$ and ${}^{n+1}\mathbf{K}^{(i-1)}$ are

$$M_{IJ} = \int_V N_I N_J dV\,, \qquad {}^{n+1}K_{IJ} = \int_V {}^{n+1}D^{(i-1)} N_{I,k} N_{J,k} dV \qquad (3)$$

Here, N_I and N_J are the interpolation functions for nodes *I* and *J*, $N_{I,k} \equiv \partial N_I / \partial x_k$, and *V* is the element volume; $\mathbf{C}$ is the nodal concentration vector; $\mathbf{Q}^S$ is the surface flux nodal vector; the left upper indices n and $n+1$ denote start and end of time step; and the right upper index *i* is the equilibrium iteration counter. The time integration scheme is implicit since the iterations lead to satisfying the equilibrium equations at the end of the time step, which is very important for the solution accuracy. Note that the summation over the repeated index k ($k = 1,2,3$) is implied. These element equilibrium equations are summed to form balance equations for the entire FE model, and the appropriate boundary conditions are implemented. For the nDS model, boundary conditions include no-flux through the symmetry planes and known concentrations ${}^{n+1}C_{in}^{(i-1)}$ and ${}^{n+1}C_{out}^{(i-1)}$ at the inlet and outlet boundaries, evaluated from change of concentration within the inlet and outlet reservoirs. The concentration changes within the reservoirs are due to mass loss (inlet reservoir) and the mass inflow (outlet reservoir).

We take into account that the diffusion coefficient depends on concentration, and ${}^{n+1}D^{(i-1)}$ in the above equation corresponds to concentration ${}^{n+1}c^{(i-1)}$ at a point within the finite element, calculated during the time integration procedure. In the Results section $D(c)$ is specified for the selected solution examples. Figure S7 shows a schematic of the FEA mesh for the nDS membrane and the user interface for the developed FEA software.

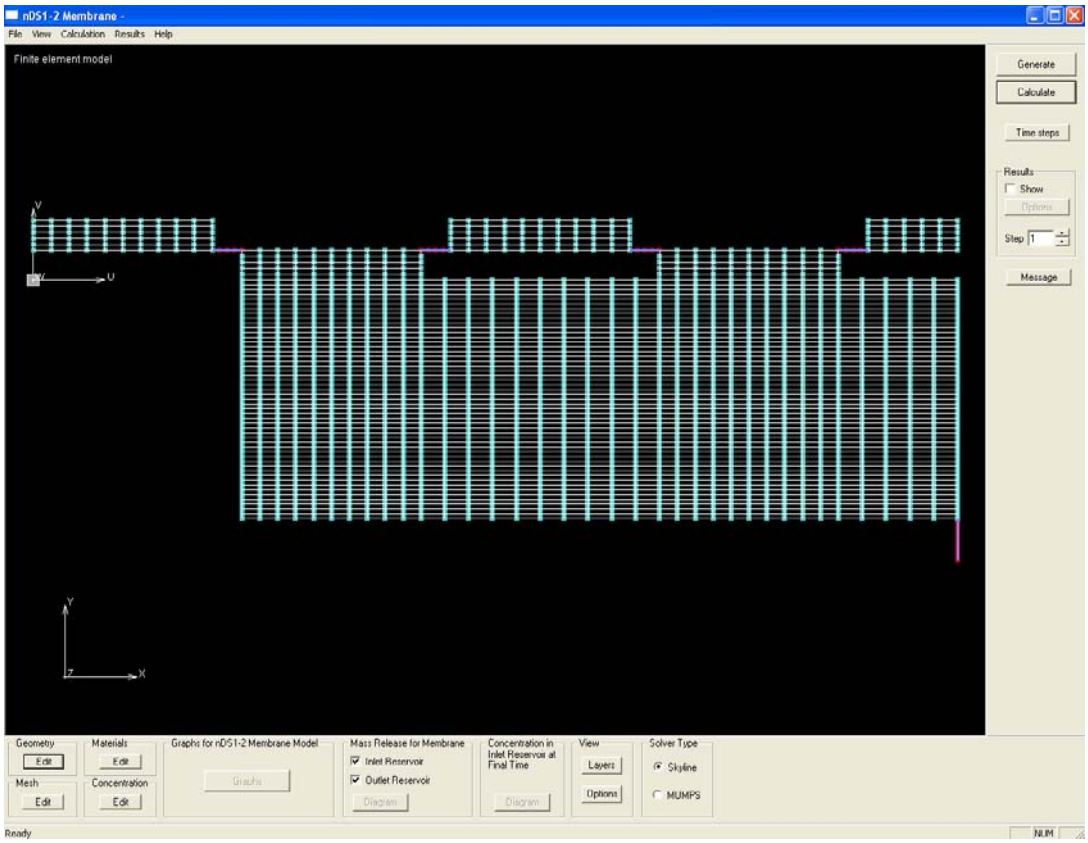

Figure S7. Schematic of the FEA mesh for the nDS membrane and user interface for the developed FEA software.

Further Acknowledgments

The authors would also like to thank the following individuals:

Mr. Paul Sadlek, Mr. Dwarakanath Geerpuram, and Mr. Brad Reelfs at Plasma-Therm, LLC., St. Petersburg, FL,

Mr. Tian Tang and Mr. Karl White at EV Group, Tempe, AZ,

Dr. Marylene Pallard at the Microelectronics Research Center, University of Texas at Austin, Austin, TX,

Mr. Wallace Martin, Dr. Gordon Pollack, Dr. Roger Robbins, Mr. Arnold Duenes, and Mr. Scott Riekena at the Cleanroom Research Laboratory, University of Texas at Dallas, Dallas, TX,

Mr. Meredith Metzler, Mr. Vince Genoa, Dr. Rob Ilic, Mr. John Grazul, Mr. Daron Westly, Mr. Michael Skvarla, and Mr. Dan Woodie at the Cornell Nanofabrication Facility, Cornell University, Ithaca, NY,

Mr. Noah Clay and Mr. John Tsakirgis at the Center for Nanoscale Systems, Harvard University, Cambridge, MA,

Dr. Mary Tang at the Stanford Nanofabrication Facility, Stanford University, Palo Alto, CA,

Dr. William M. Lackowski (formerly of), and Mr. Michael Tiner at the Center for Nano and Molecular Sciences, University of Texas at Austin, Austin, TX,

Erika Zabre for her support in the experimental analysis,

Dr. William Neil Everett and Mr. Ciro Chiappini for useful discussions and editing acumen.

Supplementary References

1. A. R. Spurr, *J. Ultrastruct. Res.*, 1969, **26**, 31-43.
2. A. Grattoni, E. De Rosa, S. Ferrati, Z. Wang, A. Gianesini, X. Liu, F. Hussain, R. Goodall, and M. Ferrari, *J. Micromech. Microeng.*, 2009, **19**, 115018.
3. M. Kojić, N. Filipović, B. Stojanović, and N. Kojić, *Computer Modeling in Bioengineering: Theoretical background, examples and software*, John Wiley & Sons, 2008.